*RevMexAA (Serie de Conferencias)*, **27**, 210–215 (2007)

# DOES LOW FREQUENCY X-RAY QPO BEHAVIOR IN GRS 1915+105 INFLUENCE SUBSEQUENT X-RAY AND INFRARED EVOLUTION?

Valerie J. Mikles,[1] Stephen S. Eikenberry,[1] and David M. Rothstein[2]

RESUMEN

Con observaciones del *Rossi X-ray Timing Explorer* examinamos el comportamiento de las oscilaciones cuasi periódicas (OCPs) durante mínimos con espectros duros en los rayos X de GRS 1915+105 acompañados de ráfagas en infrarrojo. De las doce curvas de luz que examinamos, nueve son de clase $\beta$ y 3 de clase $\alpha$, siguiendo la clasificación de Belloni et al. (2000). En la mayoría de los casos, la frecuencia de la OCP está correlacionada con el flujo en la componente de ley de potencia, lo que contradice algunas afirmaciones anteriores que la ligaban a la componente del flujo en cuerpo negro. En varios casos, la evolución de la OCP parece desacoplarse de la evolución espectral. Las curvas de luz de clase $\beta$ que muestran la correlación pueden ser distinguidas de aquellas que no lo hacen a través de la morfología del pico inicial. Hemos dividido las doce curvas de luz en base a la evolución de la OCP, la morfología del pico inicial y la intensidad de la ráfaga en IR. Concluimos que estos grupos no son modos únicos, sino que representan un continuo de comportamientos de la acreción. Creemos que el comportamiento de la OCP y la disminución de la componente espectral más energética pueden servir para predecir el estado espectral final, así como la evolución de la rafaga en IR.

ABSTRACT

Using observations with the *Rossi X-ray Timing Explorer*, we examine the behavior of $2-10$ Hz quasi-periodic oscillations (QPOs) during spectrally-hard dips in the X-ray light curve of GRS 1915+105 that are accompanied by infrared flares. Of the twelve light-curves examined, nine are $\beta$-class and three are $\alpha$-class following the scheme of Belloni et al. (2000). In most cases, the QPO frequency is most strongly correlated to the power law flux, which partially contradicts some earlier claims that the strongest correlation is between QPO frequency and blackbody flux. Seven $\beta$-class curves are highly correlated to blackbody features. In several cases, the QPO evolution appears to decouple from the spectral evolution. We find that $\beta$-class light-curves with strong correlations can be distinguished from those without by their "trigger spike" morphology. We divide the twelve $\alpha$- and $\beta$-class light-curves into three groups based on the evolution of the QPO, the morphology of the trigger spike, and the infrared flare strength. An apparent crossover case leads us to conclude that these groups are not unique modes but represent part of a continuum of accretion behaviors. We believe the QPO behavior at the initiation of the hard dip can ultimately be used to determine the terminating X-ray behavior, and the following infrared flaring behavior.

*Key Words:* **ACCRETION, ACCRETION DISKS — BLACK HOLE PHYSICS — STARS: INDIVIDUAL (GRS 1915+105) — STARS: OSCILLATIONS**

© 2007: Instituto de Astronomía, UNAM - Triggering Relativistic Jets - Supplement
Ed. William H. Lee & Enrico Ramírez-Ruiz

## 1. INTRODUCTION

Discovered in 1992 by Castro-Tirado, Brandt, & Lund (1992), GRS 1915+105 is an X-ray transient that continues to intrigue us with its unique array of variability on many wavelengths and timescales. Dubbed a microquasar because of its apparent superluminal jets (Mirabel & Rodriguez 1994), GRS 1915+105 is a black hole candidate and X-ray binary. Although it suffers $\sim 20-30$ magnitudes of extinction at visible wavelengths, GRS 1915+105 has shown great activity in the radio, infrared, and X-ray regimes. It is well-established that the spectrally-hard dips that frequently appear in the X-ray light-curves of GRS 1915+105 are associated with infrared and radio flares (Eikenberry et al. 1998; Mirabel et al. 1998; Fender & Pooley 1998; Klein-Wolt et al. 2002). These spectrally-hard dips are also associated with $2-10$ Hz variable quasi-periodic oscillations (QPOs). Belloni et al. (2000) defines a total of twelve X-ray light-curve classes for GRS 1915+105, distinguishable by general appearance, count rate, and X-ray color (related to hardness). We study the $\alpha$- and $\beta$-class light-curves in the $2-25$ keV range. Both have extended spectrally-hard dips but the length of the $\alpha$-class hard dip is nearly twice the length of

[1]Department of Astronomy, University of Florida, USA.
[2]Department of Astronomy, Cornell University, USA.

© 2007: Instituto de Astronomía, UNAM - Triggering Relativistic Jets - Supplement
Ed. William H. Lee & Enrico Ramírez-Ruiz

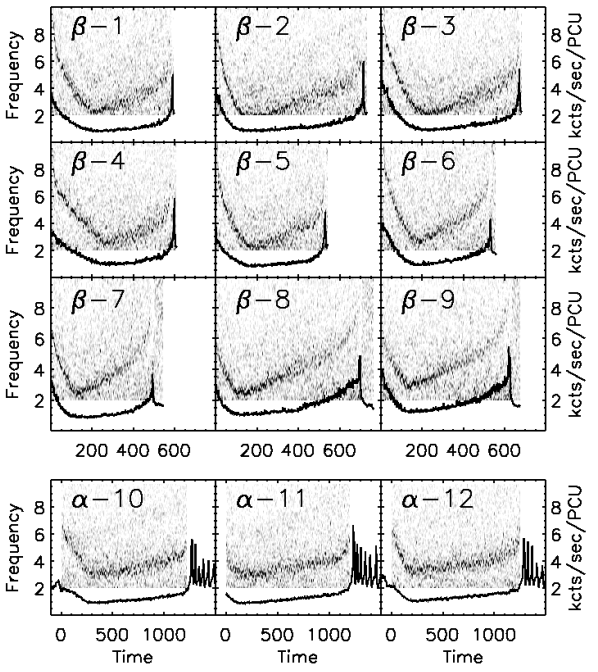


Fig. 1. A gray-scaled, fine-binned power density spectrum for the light-curves. We plot the 1-second resolution light-curve over the PDS. Note that, in the $\beta$-8 and $\beta$-9 cases, a strong low-frequency noise component appears $\sim$100 seconds before the spike.

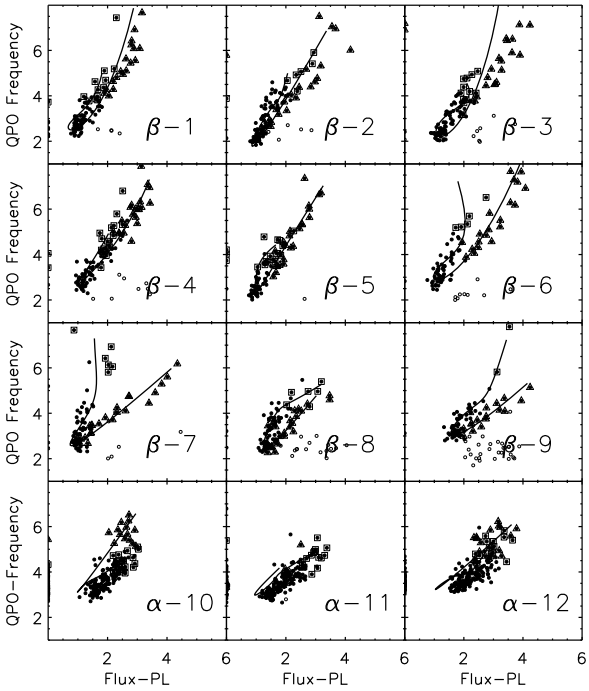


Fig. 2. Scatter plots of QPO frequency (in Hz) with power law flux, Flux-PL, (in $10^{-8} erg\ cm^{-2} s^{-1}$) for $\alpha$- and $\beta$-class light-curves. Triangles indicate detections in the first 100 seconds of entering the dip. Squares are points within the last 100 seconds before exiting the dip. The line is a fourth-order best fit to the time evolution of the features. Note that for $\beta$-1 through $\beta$-5, a strong linear correlation is apparent. For $\beta$-6, $\beta$-7, and $\beta$-9, the correlation weakens and we see different degrees of hysteresis. The open circles (non-detections of the QPO) do not contribute to the apparent hysteresis pattern. This is evidence that a continuum of QPO behaviors exists within the $\beta$-class light-curves. In $\alpha$-class light curves, a correlation exists over a smaller range of frequencies as well.

the $\beta$-class. In both the $\alpha$- and $\beta$-classes, simultaneous X-ray and infrared observations show infrared flares rising as the hard X-ray dip ends (Eikenberry et al. 1998; Mirabel et al. 1998; Rothstein, Eikenberry, & Matthews 2005). The difference between the dip/flare cycles associated with $\alpha$- vs. $\beta$-class curves is the presence of a large primary infrared flare which is uniquely associated with $\beta$-class X-ray light-curves. The sequence of a spectrally-hard dip then an infrared flare is generally associated with a plasma ejection from the source.

In this review, we examine the behavior of the QPO during the hard dip and the relationship of its behavior to subsequent infrared flares. These results are expounded upon in an article be published in the Astrophysical Journal (currently available on astro-ph/0510061).

## 2. OBSERVATIONS

We use several *Rossi X-ray Timing Explorer* (RXTE) observations of GRS 1915+105 taken on 14 - 15 August 1997, 9 September 1997, and 27 - 28 July 2002. We examine 12 regions in this work; nine of them are $\beta$-class and three are $\alpha$-class (Belloni et al. 2000). They are numbered sequentially $\beta$-1 through $\beta$-9 and $\alpha$-10 through $\alpha$-12. We fit the spectra with a combination of absorbed multi-temperature disk blackbody and power law models. Next, we calculate the power density spectrum (PDS) and track the peak frequency at 4-second resolution (see e.g. Ransom, Eikenberry, & Middleditch 2002). In Figure 1, we show a gray-scaled fine-binned PDS and overplot a one-second resolution light-curve. We determine the QPO frequency by fitting a Moffat function to the PDS in the $2 - 10$ Hz frequency range (Moffat 1969). The QPO is considered detected if it has a quality factor $Q = \nu / FWHM > 2$, where $\nu$ is the centroid frequency of the Moffat and $FWHM$ is the full-width at half max.

TABLE 1

LINEAR PEARSON CORRELATION COEFFICIENTS

| ID | Group[a] | TF[b] | BBN[c] | BBF[d] | BBT[e] | PLN[f] | PLF[g] | PLI[h] |
|---|---|---|---|---|---|---|---|---|
| $\beta$-1 | 1 | 0.96 | −0.62 | 0.84 | 0.87 | 0.87 | 0.92 | 0.52 |
| $\beta$-2 | 1 | 0.93 | −0.63 | 0.76 | 0.86 | 0.87 | 0.91 | 0.58 |
| $\beta$-3 | 1 | 0.96 | −0.62 | 0.84 | 0.90 | 0.81 | 0.88 | 0.39 |
| $\beta$-4 | 1 | 0.96 | −0.66 | 0.89 | 0.89 | 0.88 | 0.94 | 0.44 |
| $\beta$-5 | 1 | 0.96 | −0.57 | 0.86 | 0.85 | 0.90 | 0.93 | 0.62 |
| $\beta$-6 | 2 | 0.90 | −0.53 | 0.89 | 0.88 | 0.79 | 0.78 | 0.53 |
| $\beta$-7 | 2 | 0.76 | −0.42 | 0.78 | 0.75 | 0.63 | 0.59 | 0.56 |
| $\beta$-8 | 2 | 0.84 | −0.40 | 0.54 | 0.63 | 0.68 | 0.75 | 0.40 |
| $\beta$-9 | 2 | 0.87 | −0.36 | 0.67 | 0.63 | 0.76 | 0.74 | 0.39 |
| $\alpha$-10 | 3 | 0.90 | −0.10 | 0.73 | 0.48 | 0.67 | 0.77 | 0.47 |
| $\alpha$-11 | 3 | 0.87 | −0.11 | 0.57 | 0.31 | 0.74 | 0.83 | 0.46 |
| $\alpha$-12 | 3 | 0.87 | −0.11 | 0.63 | 0.43 | 0.64 | 0.75 | 0.41 |

[a]Groups are as defined in the text.

[b]Total Flux.

[c]Blackbody Normalization.

[d]Blackbody Flux.

[e]Blackbody Temperature.

[f]Power law Normalization.

[g]Power law Flux.

[h]Power law Index.

© 2007: Instituto de Astronomía, UNAM - Triggering Relativistic Jets - Supplement
Ed. William H. Lee & Enrico Ramírez-Ruiz

## 3. DISCUSSION

### 3.1. *QPO Correlation with Spectral Features*

For each hard dip, we calculate the Linear Pearson Correlation Coefficient, $r$, between the QPO frequency and various spectral features. We define events with $|r| > 0.70$ as highly correlated. We list the correlation coefficients for the twelve dips in Table 2. Figure 2 shows a scatter plot of the QPO frequency versus the power law flux for the twelve cases. The points marked with triangles are detections within the first 100 seconds of the dip and the squares are from the last 100 seconds of the dip. The line is based on a fourth order fit to the time evolution of the QPO frequency and the power law flux, tracing the approximate path of the evolution. The open circles are power peaks between 2 and 10 Hz where a QPO was not detected.

In $\beta$-1 through $\beta$-5 (August 1997) the evolution of the QPO-power law flux relation is generally tighter and the correlations stronger ($r \geq 0.80$). The $\alpha$-10 through $\alpha$-12 curves also show a tight correlation, though the QPO frequency varies over a smaller range of frequencies. In three cases, $\beta$-6, $\beta$-7, and $\beta$-9, we notice a hysteresis effect, observed as a separation between the entrance (triangles) and exit (squares) points of the dip. In the $\beta$-7 case, the hysteresis is extreme. The squares which trace the last 100 seconds of the dip show the QPO frequency rising sharply while the power law flux is relatively constant, suggesting a decoupling of the features.

Previous studies have shown that the QPO is most strongly tied to the thermal disk component (Markwardt, Swank, & Taam 1999; Feroci et al. 1999; Muno, Morgan, & Remillard 1999). Using the September 1997 data (our $\beta$-6 through $\beta$-9), Markwardt, Swank, & Taam (1999) point out that the correlation to disk flux is strongest when the QPO frequency is above 4 Hz. While this is true, the QPO frequency is in this range less than 25% of the time, and mostly falls into this range when entering or exiting the hard dip. During the course of the hard dip, the QPO will change significantly while the blackbody flux remains relatively constant. We argue that the correlation to the power law com-

© 2007: Instituto de Astronomía, UNAM - Triggering Relativistic Jets - Supplement
Ed. William H. Lee & Enrico Ramírez-Ruiz

ponent may be more fundamental, since the power law flux is more strongly tied to the X-ray emission at this point and the disk component is vanishingly small. In addition, the $\alpha$-class curves show a consistently strong correlation to the power law flux and less consistent correlation to blackbody features. We note that the bulk of the QPO change occurs during the entry into and exit from the dip. While in the dip, the spectral features remain fairly stable. Thus much of the correlation strength is tied to QPO stability during the dip and the relatively short motion at the start and end of the dip.

### 3.2. *QPO Time Behavior*

Noting the hysteresis in the QPO frequency versus power law flux distribution in several of the $\beta$-class light curves, it is likely that the spectral evolution is intimately tied to the QPO time evolution. Based on observable variations in the time evolution, we divide the light-curves into three broad groups:

- **Group 1**: An example of the $\beta$-class light-curves, a series of X-ray oscillations calm into a low, spectrally-hard dip within about 100 seconds. During this time, a QPO arises at $\sim 6-8$ Hz. Following the intensity drop of the light-curve and more specifically the power law flux, the QPO falls steadily to $\sim 2$ Hz. It remains at this frequency for over 150 seconds, after which the power law flux and QPO frequency begin a slow rise. The U-shaped QPO vanishes after the X-ray trigger spike. The total length of the dip is on the order of 600 seconds, and $\sim 30\%$ of that time is spent at the minimum frequency.

- **Group 2**: This group is also composed of $\beta$-class light-curves with similar spectral behavior to Group 1. However, the QPO behavior in this group is somewhat different. While in Group 1, the QPO falls off to $\sim 2$ Hz and lingers, in Group 2 the QPO immediately starts to rise again. While the Group 1 events remain near the minimum frequency for $> 150$ seconds, the Group 2 events remain for $< 100$ seconds (about 15% of the dip length). The following rise in frequency is the start of the hysteresis in the QPO frequency — power law flux scatter plot (Fig. 2) and likely indicates that the QPO and power law flux have decoupled. In addition, these cases see the rise of a low frequency noise component above 2 Hz as the QPO weakens in amplitude and rises rapidly in frequency. It is possible that what we identify as low-frequency noise represents an increase in rapid, unresolved QPO oscillations. The difference in behaviors in the first two groups is most remarkable because their X-ray light-curves and spectral behaviors are so similar.

- **Group 3**: The final group contains the $\alpha$-class light-curves. In these events, the hard dip is surrounded by X-ray oscillations but no independent terminal spike is observed. The total length of the dip is $\sim 1200$ seconds and the QPO disappears when the dip ends. This case is similar in shape to Group 1 QPO evolution, though twice as long. It differs in that on entering the dip the QPO frequency levels off at $\sim 3$ Hz. Overall, the frequency varies over a smaller range than seen in the other two groups.

### 3.3. *Differing Trigger Spike Morphology in $\beta$-class Light-Curves*

In addition to varying correlation behaviors, we note that the intensity and morphology of the spike varies between $\beta$-class events. Figure 3 shows a one-second resolution light-curve for each of the nine observed spikes in a time range of 55 seconds before and after the maximum. The line is a Gaussian fit to the data. In most aspects of the fit, the $\beta$-1 through $\beta$-5 (Group 1) and $\beta$-6 through $\beta$-9 (Group 2) data have different properties.

- The Group 1 data have a higher normalized amplitude.

- The Group 1 data are more symmetric while the Group 2 data shows a sharp cut-off after the peak flux (see Fig. 3).

- The Group 1 data spikes are narrower.

- The underlying slope of the light-curve is positive in the Group 1 data and flat or negative in the Group 2 data.

### 3.4. *Infrared Flaring Behavior*

Simultaneous infrared coverage is available for four out of five of our Group 1 data sets. Eikenberry et al. (1998) show that these dip/spike pairs are usually followed by large infrared flares. The events observed ranged from $\sim 60$ to 200 mJy. Although the rise and fall of the flare does not correspond to the period of X-ray oscillation, a weak infrared excess which lasts throughout the period of the X-ray oscillations is observed. Eikenberry et al. (2000) and Rothstein, Eikenberry, & Matthews (2005) explain

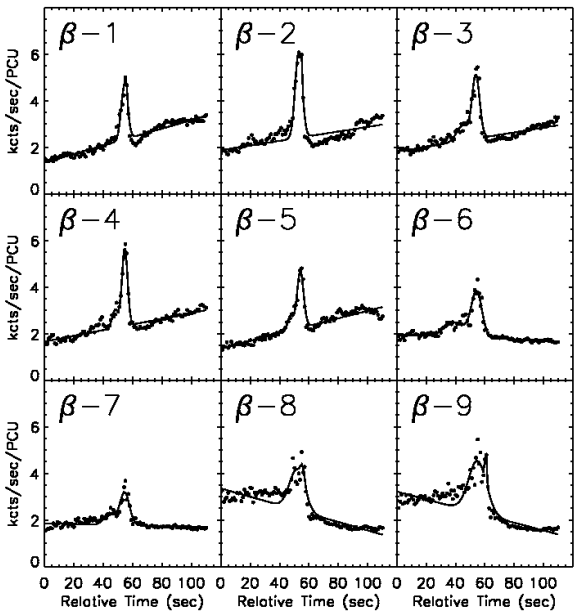


Fig. 3. The trigger spike of the $\beta$-class light-curves for 1997 August ($\beta$-1 through $\beta$-5) and 1997 September ($\beta$-6 through $\beta$-9) data at one-second time resolution. The solid lines are a double Gaussian plus polynomial fit to the data points. We classify the $\beta$-1 through $\beta$-5 events as Group 1. These have a strong, narrow, symmetric spike and the underlying flux has a positive slope. The $\beta$-6 through $\beta$-9 data we classify as Group 2 events. These have weaker, wider, asymmetric spikes and the underlying slope is flat or negative.

this excess as the superposition of many faint infrared flares each on the order of $\sim$ 10 mJy. The dominant infrared flare is associated with the X-ray trigger spike. Mirabel et al. (1998) observed a single infrared flare event associated with our $\beta$-7 curve which reached an amplitude of $\sim$ 30 mJy. Simultaneous infrared coverage is not available for the other hard dips in Group 2. In all three Group 3 light-curves of July 2002, the hard dip is followed by a $\sim$ 30 mJy infrared flare. Rothstein, Eikenberry, & Matthews (2005) showed that the $\sim$ 30 mJy flares can be explained as a summation of $\sim$ 10 mJy subflares, each associated with a soft X-ray flare.

When comparing these events, we cannot ignore the fact that all these hard dips are followed by an infrared flare, the strength of which may be tied to the presence or absence of a terminating spike. Furthermore, the shape of the spike is tied to the behavior of the QPO during the preceding dip. Therefore, the properties of the QPO appear to be fundamental for determining the subsequent jet activity in GRS 1915+105, and the question becomes, "If all hard dips start relatively the same (with the appearance of a QPO), why don't all hard dips end the same?" The Group 1 events have strong, symmetric trigger spikes and strong $\sim$ 100 mJy infrared flares. The relatively weak trigger spike and $\sim$ 30 mJy flare observed in September 1997 may be evidence that a weaker trigger spike would be associated with a weaker primary flare.

On a final note, what we have referred to as the "trigger spike" of the $\beta$-class is so named because it coincides with the start of the infrared flare. However, observations of several $\beta$-class events by Eikenberry et al. (1998) were unable to conclusively determine whether the infrared flare began simultaneously with the trigger spike. Also, in looking at the Mirabel et al. (1998) event corresponding to our $\beta$-7, one might believe that the infrared flare starts $100 - 200$ seconds PRIOR to the spike (see Mirabel et al. 1998, their Figure 3). Noting that the QPO also significantly weakens compared to the low frequency noise component $100 - 200$ seconds prior to the spike (see Fig. 1) suggests that the *origin* of the infrared flare may be causally linked to the mechanism powering the QPO, and not tied initially to the soft X-ray flaring or trigger spike. This suggests that the QPO is tied to a multi-wavelength energy release or the formation of multi-wavelength features.

### 3.5. *A Cause And Effect Summary*

While the nature of the QPO is still uncertain, it does reflect and may possibly be used to predict observable outcomes. In all of these cases, a QPO appears when the X-ray energy changes from soft to hard. While the change in hardness occurs very quickly, the flux drops slowly for $\sim$ 100 seconds. The QPO, initially around 6 Hz, falls with similar smoothness. This is where the tracks diverge. We believe that the QPO behavior at the divergent point can ultimately be used to predict how the dip will end. Consider the three groups we identify, summarized in terms of cause and effect:

- **Group 1**: A $\beta$-class light-curve enters a hard dip phase. The QPO falls off to 2 Hz and maintains that frequency for $> 150$ seconds.
  **END RESULT**:
  - The QPO frequency is tightly correlated to both blackbody and power law spectral features and the correlation lasts the length of the dip.
  - The dip lasts $500 - 700$ seconds and terminates with a strong, narrow, symmetric spike and increasing underlying flux.

© 2007: Instituto de Astronomía, UNAM - Triggering Relativistic Jets - Supplement
Ed. William H. Lee & Enrico Ramírez-Ruiz

© 2007: Instituto de Astronomía, UNAM - Triggering Relativistic Jets - Supplement
Ed. William H. Lee & Enrico Ramírez-Ruiz

  - A strong infrared flare of strength $\sim 100$ mJy follows.

- **Group 2**: A $\beta$-class light-curve enters a hard dip phase. The QPO falls off to 2 Hz, but begins increasing after $< 100$ seconds.
  **END RESULT**:
  - The QPO frequency decouples from the spectral features and the strength of the correlation is related to the degree of hysteresis.
  - The dip lasts $500 - 700$ seconds and terminates with a weak, wide, asymmetric spike and flat or decreasing underlying flux.
  - A slightly weaker infrared flare of strength $\sim 30$ mJy follows, possibly starting with the weakening of the QPO.

- **Group 3**: An $\alpha$-class light-curve enters a hard dip phase. The QPO falls off to 3 Hz and maintains that frequency for several hundred seconds.
  **END RESULT**:
  - The QPO is correlated to power law features but not to blackbody features.
  - The dip lasts $\sim 1200$ seconds and then immediately enters a period of oscillation.
  - A series of weak infrared flares with summed amplitude $\sim 10 - 30$ mJy follows and is associated with the duration of the X-ray oscillations.

## 4. CONCLUSIONS

In conclusion, we have identified three groups of hard dips with a range of spectral behavior, QPO frequency evolution, trigger spike morphology, and infrared flare strength. Each hard dip is associated with a variable low frequency QPO and is followed by an infrared flare indicating an ejection event. Similarities in the X-ray light-curve, X-ray hardness, and infrared flaring suggest that a similar mechanism is responsible for these behaviors.

While it is easy to expect different behavior from $\alpha$- and $\beta$-class light-curves, it is surprising to find differences within the $\beta$-class itself. Most interesting is the spectrum of QPO time evolution behaviors seen in our small set of observations and the fact that only a slight variation is necessary to affect the end result. The correlation of the QPO to X-ray spectral features hinges on the time evolution of the QPO. The time evolution is also intimately tied to the trigger spike morphology and subsequent infrared flaring. By studying these events together, we may better understand the underlying mechanism of plasma ejection.

V. J. M. and S. S. E. are supported in part by an NSF CAREER Award (AST-0328522). V. J. M. is also supported by a University of Florida Alumni Fellowship. D. M. R. is supported by a National Science Foundation Graduate Research Fellowship. This research has made use of data obtained from the High Energy Astrophysics Science Archive Research Center (HEASARC), provided by NASA's Goddard Space Flight Center.

## REFERENCES

Belloni, T., Klein-Wolt, M., Méndez, M., van der Klis, M., & van Paradijs, J. 2000, A&A, 355, 271
Castro-Tirado, A. J., Brandt, S., & Lund, N. 1992, IAU Circ., 5590, 2
Eikenberry, S. S., Matthews, K., Morgan, E., Remillard, R. A., & Nelson, R. W. 1998, ApJ, 494, L61
Eikenberry, S. S., Matthews, K., Muno, M., Blanco, P. R., Morgan, E. H., & Remillard, R. A. 2000, ApJ, 532, L33
Fender, R. P., & Pooley, G. G. 1998, MNRAS, 300, 573
Feroci, M., Matt, G., Pooley, G. G., Costa, E., Tavani, M., & Belloni, T. 1999, A&A, 351, 985
Klein-Wolt, M., Fender, R. P., Pooley, G. G., Belloni, T., Migliari, S., Morgan, E. H., van der Klis, M. 2002, MNRAS, 331, 745
Markwardt, C. B., Swank, J. H., & Taam, R. E. 1999, ApJ, 513, L37
Mirabel, I. F., Dhawan, V., Chaty, S. Rodríguez, L. F., Martí, J., Robinson, C. R., Swank, J., & Geballe, T. R. 1998, A&A, 330, L9
Mirabel, I. F. & Rodríguez, L. F. 1994, Nature, 371, 46
Moffat, A. F. J. 1969, A&A, 3, 455
Muno, M. P., Morgan, E. H., & Remillard, R. A. 1999, ApJ, 527, 321
Ransom, S. M., Eikenberry, S. S., & Middleditch, J. 2002, ApJ, 124, 1788
Rothstein, D. M., Eikenberry, S. S., & Matthews, K. 2005, ApJ, 626, 991

Valeri J. Mikles and Stephen S. Eikenberry: Department of Astronomy, University of Florida, Gainesville, FL 32611, USA (mikles@astro.ufl.edu).
David M. Rothstein: Department of Astronomy, Cornell University, Ithaca, NY 14853, USA.